FULL PAPER

Oxygen Vacancies and Ordering of d-levels Control Voltage Suppression in Oxide Cathodes: the Case of Spinel $LiNi_{0.5}Mn_{1.5}O_{4-\delta}$

*Peter V. Sushko, Kevin M. Rosso, Ji-Guang Zhang, Jun Liu, and Maria L. Sushko**

This study presents a microscopic model for the correlation between the concentration of oxygen vacancies and voltage suppression in high voltage spinel cathodes for Li-ion batteries. Using first principles simulations, it is shown that neutral oxygen vacancies in $LiNi_{0.5}Mn_{1.5}O_{4-\delta}$ promote substitutional Ni/Mn disorder and the formation of Ni-rich and Ni-poor regions. The former trap oxygen vacancies, while the latter trap electrons associated with these vacancies. This leads to the creation of deep and shallow Mn^{3+} states and affects the stability of the lattice Li ions. Together, these two factors result in a characteristic profile of the voltage dependence on Li content. This insight provides guidance for mitigating the voltage suppression in $LiNi_{0.5}Mn_{1.5}O_4$ and other cathodes.

1. Introduction

Spinel transition metal oxides (general formula AB_2O_4) form a large class of materials with diverse properties and potential applications as high-voltage cathodes for Li-ion batteries,[1,2] transparent conductors,[3–5,6] and superconductors.[7] However, their electrical properties remain poorly understood, hindering knowledge-based design of compositions with desired performance characteristics. Electrical properties of these oxides are largely determined by the ability of the transition metal ions, which have partially filled 3d orbitals, to change their oxidation states, a degree of freedom widely exploited in design. For example, doping is often used to introduce mixed valence states in the transition metals and, thus, tune the material's conductivity.[8] Doping not only controls the electronic transport in spinels, but also influences ionic transport of the A-type cations, as revealed in extensive experimental studies of spinel cathode materials used in Li-ion batteries.[9–13] Another common feature of doped spinel transition metal oxides is a close connection between their electrical and magnetic properties on the one side and the details of cation arrangement in the lattice on the other. Several studies addressing the origin of cation ordering in stoichiometric spinel oxides have been reported.[14,15] Cation doping and the presence of defects in the anion sublattice, oxygen vacancies being the most common one,[16] add a new level of complexity into the structure–property relation in these materials; such effects remain poorly understood. Defects trigger changes in the electronic structure of complex transition metal oxides, thus, affecting, the energetics for electron and ion transport. The intimate link between the local geometrical structure of defects and macroscopic electric properties presents a challenge for materials design: improving the ionic and electronic transport properties and stability of the electrochemical performance using the trial-and-error approach alone is a daunting task, as manifested, for example, by the voltage suppression problem in Li-Mn-rich oxides, solution for which remains elusive.

Here, we investigate the relation between the details of cation arrangement and electrical properties of transition metal spinel oxides on the example of oxygen-deficient (i.e., reduced) spinel $LiNi_{0.5}Mn_{1.5}O_{4-\delta}$ (LNMO), presently one of the most promising cathode materials for the next generation Li-ion batteries. Electrochemical performance of stoichiometric and oxygen-deficient LNMO with ordered and disordered configurations of Ni has been extensively investigated.[1,9,10,12,17–39] It was experimentally shown that Ni/Mn site disorder increases the specific capacity and conductivity of LNMO.[10] Similarly, theoretical evidence suggests that cation disorder lowers the Li atom extraction energies.[40] Moreover, the electrochemical performance of LNMO was shown to be strongly linked to the concentration of oxygen vacancies.[41] However, the origin of this effect remains elusive. Understanding the relation between oxygen deficiency, which can be controlled during synthesis, and the electrochemical properties of transition metal oxides opens a new avenue for knowledge-based design of electrode materials.

In this study, we investigate the effect of oxygen vacancies on the arrangement of Ni and Mn cations in the lattice and on the electronic structure and electrochemical properties of LNMO using ab initio simulations based on density functional theory. We propose that i) oxygen deficiency promotes formation of disordered Ni/Mn configurations and ii) both oxygen

Dr. P. V. Sushko
Department of Physics and Astronomy
and London Centre for Nanotechnology
University College London
Gower Street, London, WC1E 6BT, UK
Dr. K. M. Rosso, Dr. J.-G. Zhang,
Dr. J. Liu, Dr. M. L. Sushko
Pacific Northwest National Laboratory
Richland, WA 99352, USA
E-mail: maria.sushko@pnnl.gov

DOI: 10.1002/adfm.201301205

deficiency and Ni/Mn site disorder are responsible for changes in Li vacancy formation energies and the corresponding voltages in $Li_xNi_{0.5}Mn_{1.5}O_{4-\delta}$ as a function of Li concentration ($0 \leq x \leq 1$). Our results provide an explanation for the origin of the voltage suppression phenomenon and suggest pathways for minimizing its detrimental effect.

2. Results and Discussion

To elucidate the effect of oxygen vacancies on the Ni/Mn ordering, we calculated relative energies of all non-equivalent Ni/Mn configurations within the 56-atom LNMO supercell using an empirical potential shell model, as described elsewhere,[10] and then refined these calculations for 10 lowest-energy configurations using the Perdew-Burke-Errizerhof revised for solids (PBEsol) density functional and the Hubbard U correction for Ni and Mn 3d states.[42] Since the electronic structure of oxygen vacancies strongly depends on their immediate environment,[16] Ni/Mn configurations in which oxygen sites have several types of nearest neighbor environments were selected. Specifically, in configuration A (the lowest energy one, $P4_332$ space group with Ni ordered over the 4b sites), O sites have either three Mn neighbors (Ni_0Mn_3) or one Ni and two Mn neighbors (Ni_1Mn_2), while in configuration B (the 3rd lowest energy one, $Fd\bar{3}m$ space group with Ni randomly occupying 16d sites), O sites have Ni_0Mn_3, Ni_1Mn_2, and Ni_2Mn_1 neighbors. Ni/Mn configurations containing oxygen sites with Ni_3Mn_0 neighbors are significantly less stable than configurations A and B and, therefore, are not considered here.

The energy difference between the stoichiometric configurations A and B is 0.76 eV per 56-atom supercell (**Table 1**). In the oxygen deficient case, this energy difference depends on the oxygen vacancy (V_O) site and becomes as low as 0.21 eV if the vacancy occupies the lowest energy sites in both A and B. The data in Table 1 confirms that i) the V_O are most likely to form at the O sites having one or more neighboring Ni ions and ii) oxygen deficiency diminishes thermodynamic preference for the formation of the lowest-energy Ni/Mn configuration, which is consistent with earlier shell model calculations.[10] Thus, oxygen deficiency promotes substitutional disorder of Ni/Mn site occupation.

In the following, we consider four systems: i) a fully stoichiometric LNMO and oxygen-deficient LNMO containing ii) one V_O–Ni_1Mn_2, iii) one V_O–Ni_2Mn_1, and iv) two neighboring

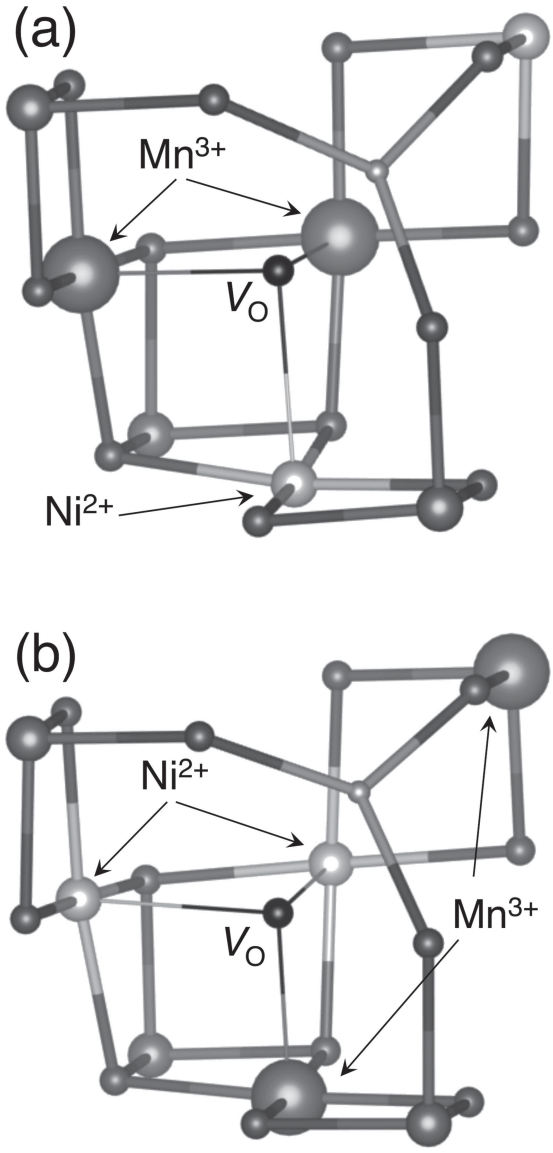

Figure 1. Local atomic structure of a neutral oxygen vacancy (V_O) at a) Ni_1Mn_2 sites and b) Ni_2Mn_1 sites. The vacancy site is shown with a small black sphere. Two electrons associated with V_O localize on nearest or second-nearest Mn ions. Lattice ions in the order of increasing size: Li^+ (light), O^{2-} (dark), Mn^{4+} (dark), Ni^{2+} (light), Mn^{3+} (dark).

Table 1. Relative energies (in eV per 56-atom supercell) of the stoichiometric and oxygen deficient Ni/Mn configurations A and B. Positive values mean that configuration A is more stable than B. The most stable vacancy sites in A and B are shown in bold.

Ni/Mn configuration		A		
	V_O site	No V_O	V_O–Ni_0Mn_3	**V_O–Ni_1Mn_2**
B	No V_O	0.76		
	V_O–Ni_0Mn_3		0.32	0.97
	V_O–Ni_1Mn_2		0.21	0.86
	V_O–Ni_2Mn_1		–0.44	0.21

V_O–Ni_2Mn_1 defects. The analysis of the charge density distribution in reduced LNMO suggests that two electrons associated with the vacancy at the Ni_1Mn_2 site localize on e_g states of the two Mn ions nearest to the vacancy (**Figure 1**a) converting them to Mn^{3+}. In the case of V_O–Ni_2Mn_1, one of these electrons localizes on the Mn site next to the vacancy and another one, at the second-nearest Mn site (Figure 1b). In both cases, the V_O site becomes depleted of electron density and acquires the effective charge of approximately +2. Since the ionic charge of Ni species is less positive than that of Mn species, regions with higher than average local concentrations of Ni carry an effective negative local charge, which explains why V_O is preferentially

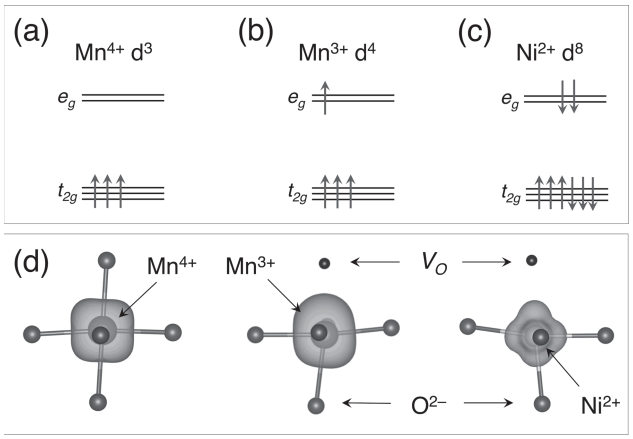

Figure 2. Schematics of the electronic structures of a) Mn^{4+}, b) Mn^{3+}, and c) Ni^{2+} ions in the stoichiometric (Mn^{4+} and Ni^{2+} only) and oxygen-deficient LNMO lattice and d) the corresponding spin-densities. The up and down arrows correspond to spin-up and spin-down electronic states, respectively.

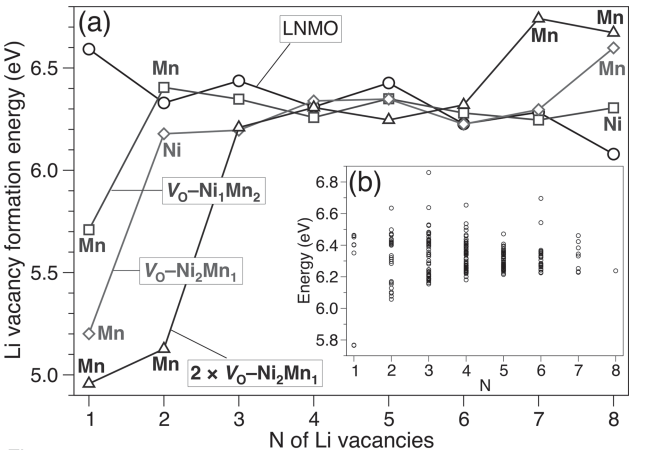

Figure 3. a) Li atom vacancy formation energies in $Li_{8-x}Ni_4Mn_{12}O_{32-y}$ (x = 0–7 and y = 0–2) calculated with respect to an isolated Li atom and shown as a function of the number of vacancies N = x + 1. The Ni and Mn symbols, where shown, indicate which atoms are oxidized upon extraction of the corresponding Li atom; Ni atoms are oxidized in all other cases. b) Li vacancy formation energies (averaged over N) for Ni/Mn configuration A containing a V_O at a Ni_1Mn_2 site.

formed in such regions. For the same reason, occupied e_g states of Mn^{3+} in Ni-rich regions have, on average, higher one-electron energies than those in Ni-poor regions.

Formation of oxygen vacancies promotes occupation of the Mn e_g states (**Figure 2**) and, thereby, induces redistribution of the charge density and moves the energy of the highest occupied state of the LNMO lattice to higher values. In addition, the effective positive charge of the vacancies reduces the binding energy of nearby Li^+ ions. These factors affect energetics for lithiation/de-lithiation, which, as we show below, is consistent with the characteristic profile of the voltage–capacity curves observed in reduced LNMO.

Figure 3a shows the formation energies of Li atom vacancies in $Li_{8-x}Ni_4Mn_{12}O_{32-y}$ (x = 0–7 and y = 0–2) calculated for the stoichiometric Ni/Mn configuration A and oxygen deficient configurations A and B with the lowest-energy V_O configurations. For each value of x, we considered all possible arrangements of a neutral Li vacancy within the Li_{8-x} sublattice, which gives a range of values for the vacancy formation energy (Figure 3b). These simulations show that energy required to extract Li atoms from the stoichiometric LNMO are approximately constant over a wide range of Li concentrations. In contrast, energy required to extract the first Li atom in the vicinity of V_O–Ni_1Mn_2 vacancy is ≈0.7 eV smaller than that needed to extract the second and all other Li atoms, while in the case of the V_O–Ni_2Mn_1 vacancy, this difference exceeds 1 eV.

Analysis of the geometrical and electronic structures of the $Li_{8-x}Ni_4Mn_{12}O_{31}$ demonstrates that at small x (x = 1 for isolated V_O and x = 1,2 for the V_O dimer) Li vacancies are formed at the sites nearest to the V_O, and the Mn^{3+} ions near the V_O are converted to Mn^{4+} states. To rationalize this effect of the V_O, we note that the main contributions to the formation energy of neutral Li vacancies come from i) the energy required to extract a Li^+ ion and ii) ionization potential of the lattice. The ionic contribution is determined by the magnitude of the positive electrostatic potential due to V_O, which destabilizes Li^+ ions next to it (see Supporting Information) and significantly lowers the Li^+ vacancy formation energy at this site. At the same time, since V_O form preferentially in the Ni-rich regions, which are negatively-charged with respect to the lattice, the energy levels of the Mn^{3+} e_g states in these regions are relatively high and, therefore, the ionization potential is low. Thus, the Ni-rich regions give rise to shallow Mn^{3+} states. Conversely, the Ni-poor regions are positively charged with respect to the lattice and the ionization potential of the Mn^{3+} e_g states in these areas is high, that is, they give rise to deep Mn^{3+} states.

The electronic structure of oxygen vacancies can be described using the density of states (**Figure 4**). Due to different local environments of Mn^{3+} ions in the first and second coordination shells of V_O, the occupied e_g states of Mn span a range of energies and can be located above the e_g band or overlap with it. For example, in the fully lithiated V_O–Ni_1Mn_2 defect (Figure 4a), e_g states of one Mn^{3+} appear above the e_g band of Ni, while in the V_O–Ni_2Mn_1 defect the e_g states of both Mn^{3+} species are just below the highest occupied Ni e_g states (Figure 4b). We note that as the charge distribution of the LNMO lattice changes in the process of delithiation, so do the positions of the occupied Mn^{3+} e_g levels. In particular, as shown in Figure 3a, extraction of the first two Li atoms in the vicinity of the V_O–Ni_1Mn_2 defect results in oxidation of both Mn^{3+} ions, that is, e_g states of both Mn^{3+} species are shallow. On the other hand, in V_O–Ni_2Mn_1 defects only 50% of the Mn^{3+} e_g states are shallow, while the other 50% appear to be deep states and get oxidized only at the very low Li concentration: x = 7 for an isolated V_O–Ni_2Mn_1 and x = 6,7 for a V_O–Ni_2Mn_1 dimer.

Since the electrostatic potential induced by V_O is proportional to $1/r$, where r is the distance from the vacancy site, it is expected that Li^+ ions located closer to V_O are affected by its electrostatic potential to a larger extent. However, given a relatively small size of the supercell, we did not find any clear correlation between the locations of the Li^+ vacancies and the V_O beyond the nearest neighbors. Indeed, outside the second

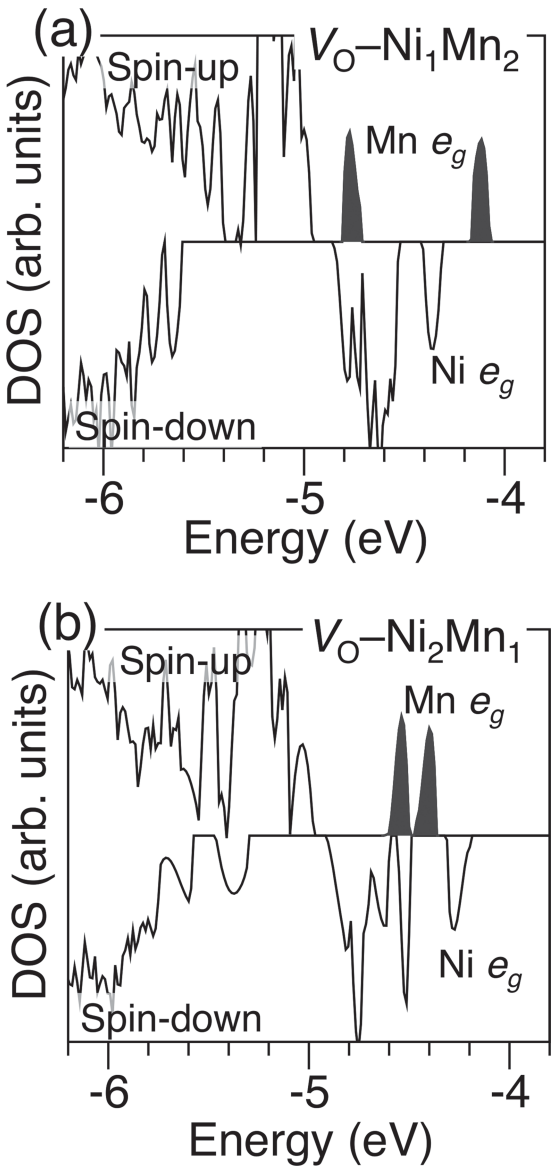

Figure 4. Densities of states for fully lithiated Ni/Mn configurations with a V_O a) at the Ni_1Mn_2 and b) Ni_2Mn_1 sites, as calculated using the hybrid B3LYP density functional (see Supporting Information). Shaded areas show the occupied e_g states of Mn^{3+} ions.

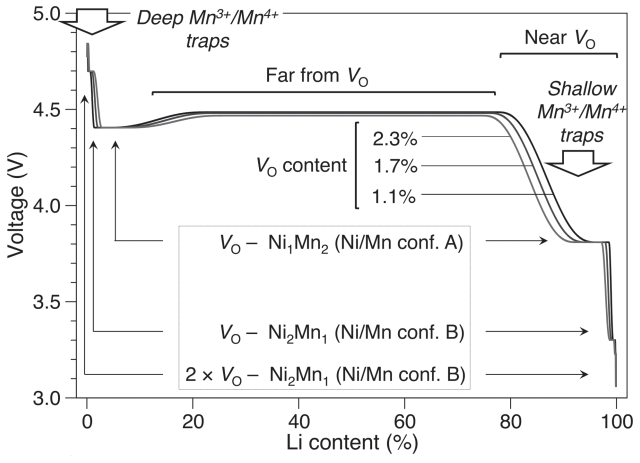

Figure 5. Voltage calculated with respect to the Li metal electrode for several concentrations of oxygen vacancies. The electrostatic potential due to the V_O and low ionization potential due to shallow Mn^{3+} states dominate at the high Li concentrations, while the high ionization potential due to deep Mn^{3+} states dominate at low Li concentrations.

coordination shell of Li atoms the electrostatic potential can be considered as a slowly varying function of r. Since for larger values of x, Li^+ vacancies are compensated by the electrons vacating the states of the relatively narrow Ni e_g band (Figure 4), its ionization energy does not change significantly with the Li concentration even though this band is gradually depleted as x increases, which explains the nearly constant Li vacancy formation energy for $x = 3$–8 in this system and in stoichiometric LNMO (Figure 3a).

The Li vacancy formation energies (Figure 3a) were converted into voltage-capacity curves as follows. First, we estimated relative concentrations of the most stable oxygen vacancy configurations from the total energy calculations of oxygen-deficient LNMO. The concentrations for an isolated V_O at Ni_1Mn_2 and Ni_2Mn_1 sites and a vacancy dimer, in which both vacancies are at Ni_2Mn_1 sites, as calculated for the processing temperature of 900 °C,[10] are 85.6%, 11.6%, and 2.8%, respectively. Then, fractions of Li atoms affected by these vacancies for any given V_O concentration were calculated assuming that Li vacancies form at the sites with the lowest vacancy formation energy first (see Supporting Information for details).

The voltage profiles calculated for three reduced LNMO samples, corresponding to Mn^{3+} concentrations of 6, 9, and 12%, are shown in **Figure 5**. The low-voltage region at high Li concentration is dominated by the Li sites that are located next to V_O and Mn with shallow Mn^{3+} states simultaneously, so as both the ionic and the electronic contributions to the cost of forming the neutral Li vacancy are small. It follows from our results that such sites are located in the locally Ni-rich regions. If LNMO is weakly oxygen deficient, formation of extensive Ni-rich regions is suppressed, and they are quickly depleted as the concentration of Li is reduced. However, if LNMO contains a large concentration of oxygen vacancies, the formation of locally Ni-rich regions becomes favorable (see Table 1) and the low-voltage region covers a noticeable interval of Li concentration. We emphasize that even in the case of the lowest energy ordered Ni/Mn configuration A, the formation of oxygen vacancies results in the voltage drop by as much as 0.6–0.7 V. However, this effect is much more pronounced if Ni/Mn site occupation allows the formation of O–Ni_2Mn_1 local structures, as it is the case in the Ni/Mn configuration B. On the other hand, in the limit of the low Li content, the electrostatic potential produced by V_O is no longer a significant factor. Instead, the Li extraction energy is determined by the lowest ionization potential of the lattice. In all our calculations, the deep Mn^{3+} states are associated with V_O–Ni_2Mn_1 defects, which result in the voltage spike of 0.4–0.5 V at $x = 1,2$ (Figure 3a). These results are consistent with the experimentally observed voltage steps at ≈90% and ≈10% Li content.[10,28,41]

The comparison of the voltage values at the high and low Li content suggests that the electronic contribution of V_O (i.e., ionization of Mn^{3+} ions) into deviation of voltage from its median value is of the order of 0.5 eV, while its ionic contribution (i.e., the effect of its electrostatic potential on the stability of neighboring Li^+ ions) is of the order of 1 eV. Importantly, ionization of Mn^{3+} ions can contribute to both lower and higher voltage if the corresponding Mn^{3+} states are shallow and deep, respectively. In turn, this suggests a pathway for minimizing the detrimental effects of the oxygen vacancies on the voltage characteristics. We propose that doping LNMO with transition metal elements that have low-lying unoccupied states can eliminate shallow Mn^{3+} states altogether and, thus, reduce voltage suppression at high Li content. Alternatively, substituting a fraction of Ni^{2+} and Mn^{4+} ions with redox-inert cations that have high ionic charges can increase stability of Li^+ ions. In this case, the electrons associated with a neutral oxygen vacancy are favored to localize at the vacancy site rather than on Mn species and, thus, mimic the Li^+–O^{2-} interaction to some extent.

3. Conclusions

Our simulations show that neutral oxygen vacancies in LNMO promote formation of Ni-rich regions, which are negatively charged with respect to the lattice. This makes the electrons associated with these vacancies to localize on Mn^{3+} e_g states of two types: shallow states in the Ni-rich regions and deep states in the Ni-poor regions. The positive electrostatic potential produced by the oxygen vacancies and the existence of the shallow and deep Mn^{3+} states result in appearance of the low-voltage region at high Li content and high-voltage region at low Li content. This is consistent with characteristic changes in the voltage capacity curves observed experimentally during electrochemical cycling.[10,43,44] We propose that doping LNMO with judiciously selected cations can help to remedy voltage suppression effects. This approach may also be used to enhance the electrochemical stability of Li–Mn rich oxides, which tend to experience continuous voltage fade.[1,12,37,45–47]

4. Experimental Section

The $LiNi_{0.5}Mn_{1.5}O_4$ lattice was represented using the crystallographic 56-atom super cell. The lattice constant has been fixed at the value, which corresponds to the experimentally observed lattice constant for LNMO, prepared using high temperature calcination, that is, 8.182 Å for the cubic super cell.[10] It was found that relaxation the lattice cell vectors changes the Li vacancy formation energies by less than 0.1% (see Supporting Information) and thereby does not give a significant contribution to the calculated voltage.

Ab initio simulations of delithiation of stoichiometric and reduced LNMO were performed using density functional theory (DFT), the PBEsol exchange-correlation functional designed for solids.[42] and projector augmented wave potentials,[48] as implemented in the VASP code.[49,50] The plane-wave basis with a 500 eV cutoff and a $2 \times 2 \times 2$ Monkhorst-Pack grid were used. In all cases, the Hubbard U correction for Ni and Mn 3d states was applied to account for the electron localization at these ions.[2]

The internal coordinates were optimized in each case. These coordinates were then used to calculate the electronic structures of the most stable configurations of oxygen- and lithium-deficient LNMO with the hybrid density functional B3LYP[51,52] and Gaussian-type basis set,[53] as implemented in the CRYSTAL package.[54,55]

It was found that the most stable spin configuration in the stoichiometric LNMO is formed by the high-spin states of Mn^{4+} ions (3 spin-up t_{2g} electrons) and Ni^{2+} ions (2 spin-down e_g electrons). This configuration was taken as a reference in all subsequent calculations of LNMO with oxygen and lithium vacancies and the number of spin-up and spin-down electrons was adjusted accordingly.

To simulate the voltage–capacity curves, the energy cost for the extraction of n ($n = 1$–8) Li atoms, were calculated quantum mechanically for all possible arrangements of Li vacancies in a 56 atom cubic cell with two lowest-energy arrangements of Ni ions and containing 0, 1, and 2 oxygen vacancies. The formation energies were adjusted for the chemical potential of the metal Li (equal to –1.9 eV) to obtain the corresponding voltage values.[2]

Supporting Information

Supporting Information is available from the Wiley Online Library or from the author.

Acknowledgements

This work was supported by the Laboratory-Directed Research and Development Program at Pacific Northwest National Laboratory (PNNL). PNNL is a multiprogram national laboratory operated for DOE by Battelle under Contract DE-AC05-76RL01830. PVS also acknowledges The Royal Society, Materials Chemistry Consortium, and EPSRC grants EP/F067496 and EP/H018328/1. Most of the simulations were performed using PNNL Institutional Computing facility.

Received: April 9, 2013
Published online: June 19, 2013

[1] J. M. Tarascon, W. R. McKinnon, F. Coowar, T. N. Bowmer, G. Amatucci, D. Guyomard, *J. Electrochem. Soc.* **1994**, *141*, 1421.
[2] B. Xu, S. Meng, *J. Power Sources* **2010**, *195*, 4971.
[3] N. Ueda, T. Omata, N. Hikuma, K. Ueda, H. Mizoguchi, T. Hashimoto, H. Kawazoe, *Appl. Phys. Lett.* **1992**, *61*, 1954.
[4] T. Omata, N. Ueda, N. Hikuma, K. Ueda, H. Mizoguchi, T. Hashimoto, H. Kawazoe, *Appl. Phys. Lett.* **1993**, *62*, 499.
[5] T. Omata, N. Ueda, K. Ueda, H. Kawazoe, *Appl. Phys. Lett.* **1994**, *64*, 1077.
[6] C. F. Windisch, K. F. Ferris, G. J. Exarhos, *J. Vac. Sci. Technol. A* **2001**, *19*, 1647.
[7] I. Hase, S. I. Ikeda, N. Shirakawa, J. K. Stalick, *J. Low Temp. Phys.* **2003**, *131*, 269.
[8] T. R. Paudel, A. Zakutayev, S. Lany, M. d'Avezac, A. Zunger, *Adv. Funct. Mater.* **2011**, *21*, 4493.
[9] R. Santhanam, B. Rambabu, *J. Power Sources* **2010**, *195*, 5442.
[10] J. Xiao, X. L. Chen, P. V. Sushko, M. L. Sushko, L. Kovarik, J. J. Feng, Z. Q. Deng, J. M. Zheng, G. L. Graff, Z. M. Nie, D. W. Choi, J. Liu, J. G. Zhang, M. S. Whittingham, *Adv. Mater.* **2012**, *24*, 2109.
[11] M. C. Yang, B. Xu, J. H. Cheng, C. J. Pan, B. J. Hwang, Y. S. Meng, *Chem. Mater.* **2011**, *23*, 2832.
[12] B. J. Hwang, Y. W. Wu, M. Venkateswarlu, M. Y. Cheng, R. Santhanam, *J. Power Sources* **2009**, *193*, 828.
[13] M. M. Thackeray, W. I. F. David, P. G. Bruce, J. B. Goodenough, *Mater. Res. Bull.* **1983**, *18*, 461.
[14] H. S. C. Oneill, A. Navrotsky, *Am. Mineral.* **1983**, *68*, 181.
[15] V. Stevanovic, M. d'Avezac, A. Zunger, *J. Am. Chem. Soc.* **2011**, *133*, 11649.

[16] A. M. Stoneham, *Theory of Defects in Solids: Electronic Structure of Defects in Insulators and Semiconductor*, Oxford University Press, New York, USA **2001**.
[17] R. Alcantara, M. Jaraba, P. Lavela, J. L. Tirado, P. Biensan, A. de Guibert, C. Jordy, J. P. Peres, *Chem. Mater.* **2003**, *15*, 2376.
[18] B. Ammundsen, J. Roziere, M. S. Islam, *J. Phys. Chem. B* **1997**, *101*, 8156.
[19] K. Ariyoshi, Y. Maeda, T. Kawai, T. Ohzuku, *J. Electrochem. Soc.* **2011**, *158*, A281.
[20] J. C. Arrebola, A. Caballero, L. Hernan, J. Morales, *J. Power Sources* **2008**, *180*, 852.
[21] T. A. Arunkumar, A. Manthiram, *Electrochem. Solid State Lett.* **2005**, *8*, A403.
[22] P. G. Bruce, B. Scrosati, J. M. Tarascon, *Angew. Chem. Int. Ed.* **2008**, *47*, 2930.
[23] J. Cabana, H. H. Zheng, A. K. Shukla, C. Kim, V. S. Battaglia, M. Kunduraci, *J. Electrochem. Soc.* **2011**, *158*, A997.
[24] X. Fang, N. Ding, X. Y. Feng, Y. Lu, C. H. Chen, *Electrochim. Acta* **2009**, *54*, 7471.
[25] J. A. Gao, J. A. J. Li, C. Y. Jiang, C. R. Wan, *J. Electrochem. Soc.* **2010**, *157*, A899.
[26] B. Kang, G. Ceder, *Nature* **2009**, *458*, 190.
[27] J. H. Kim, S. T. Myung, Y. K. Sun, *Electrochim. Acta* **2004**, *49*, 219.
[28] J. H. Kim, S. T. Myung, C. S. Yoon, S. G. Kang, Y. K. Sun, *Chem. Mater.* **2004**, *16*, 906.
[29] D. Q. Liu, J. T. Han, J. B. Goodenough, *J. Power Sources* **2010**, *195*, 2918.
[30] G. Q. Liu, L. Wen, X. Wang, B. Y. Ma, *J. Alloys Compd.* **2011**, *509*, 9377.
[31] L. W. Ma, B. Z. Chen, X. C. Shi, W. Zhang, K. Zhang, *Colloids Surf., A* **2010**, *369*, 88.
[32] B. Markovsky, Y. Talyossef, G. Salitra, D. Aurbach, H. J. Kim, S. Choi, *Electrochem. Commun.* **2004**, *6*, 821.
[33] S. H. Oh, K. Y. Chung, S. H. Jeon, C. S. Kim, W. I. Cho, B. W. Cho, *J. Alloys Compd.* **2009**, *469*, 244.
[34] K. M. Shaju, P. G. Bruce, *Dalton Trans.* **2008**, 5471.
[35] L. P. Wang, H. Li, X. J. Huang, E. Baudrin, *Solid State Ionics* **2011**, *193*, 32.
[36] H. Xia, Y. S. Meng, L. Lu, G. Ceder, *J. Electrochem. Soc.* **2007**, *154*, A737.
[37] Y. G. Xia, H. Y. Wang, Q. Zhang, H. Nakamura, H. Noguchi, M. Yoshio, *J. Power Sources* **2007**, *166*, 485.
[38] L. F. Xiao, Y. Q. Zhao, Y. Y. Yang, X. P. Ai, H. X. Yang, Y. L. Cao, *J. Solid State Electrochem.* **2008**, *12*, 687.
[39] H. Y. Xu, S. Xie, N. Ding, B. L. Liu, Y. Shang, C. H. Chen, *Electrochim. Acta* **2006**, *51*, 4352.
[40] E. Lee, K. A. Persson, *Energy Environ. Sci.* **2012**, *5*, 6047.
[41] J. M. Zheng, J. Xiao, X. Q. Yu, L. Kovarik, M. Gu, F. Omenya, X. L. Chen, X. Q. Yang, J. Liu, G. L. Graff, M. S. Whittingham, J. G. Zhang, *Phys. Chem. Chem. Phys.* **2012**, *14*, 13515.
[42] J. P. Perdew, A. Ruzsinszky, G. I. Csonka, O. A. Vydrov, G. E. Scuseria, L. A. Constantin, X. L. Zhou, K. Burke, *Phys. Rev. Lett.* **2008**, *100*, 136406.
[43] M. Kerlau, M. Marcinek, V. Srinivasan, R. M. Kostecki, *Electrochim. Acta* **2007**, *52*, 5422.
[44] K. Amine, J. Liu, I. Belharouak, S. H. Kang, I. Bloom, D. Vissers, G. Henriksen, *J. Power Sources* **2005**, *146*, 111.
[45] A. R. Armstrong, M. Holzapfel, P. Novak, C. S. Johnson, S. H. Kang, M. M. Thackeray, P. G. Bruce, *J. Am. Chem. Soc.* **2006**, *128*, 8694.
[46] J. Cabana, S. H. Kang, C. S. Johnson, M. M. Thackeray, C. P. Grey, *J. Electrochem. Soc.* **2009**, *156*, A730.
[47] M. Gu, I. Belharouak, J. Zheng, H. Wu, J. Xiao, A. Genc, K. Amine, S. Thevuthasan, D. R. Baer, J. G. Zhang, N. D. Browning, J. Liu, C. Wang, *ACS Nano* **2013**, *7*, 760.
[48] P. E. Blochl, *Phys. Rev. B* **1994**, *50*, 17953.
[49] G. Kresse, J. Furthmuller, *Phys. Rev. B* **1996**, *54*, 11169.
[50] G. Kresse, D. Joubert, *Phys. Rev. B* **1999**, *59*, 1758.
[51] A. D. Becke, *J. Chem. Phys.* **1993**, *98*, 5648.
[52] C. T. Lee, W. T. Yang, R. G. Parr, *Phys. Rev. B* **1988**, *37*, 785.
[53] T. Bredow, K. Jug, R. A. Evarestov, *Phys. Status Solidi B* **2006**, *243*, R10.
[54] CRYSTAL09 basis sets, http://www.crystal.unito.it/Basis_Sets/Ptable.html, last accessed: June **2013**.
[55] R. Dovesi, V. R. Saunders, C. Roetti, R. Orlando, C. M. Zicovich-Wilson, F. Pascale, B. Civalleri, K. Doll, N. M. Harrison, I. J. Bush, P. D'Arco, M. Llunell, *CRYSTAL09 User's Manual*, University of Torino, Torino, **2009**.